Electronic Supplementary Material (ESI) for ChemComm.

Supporting Information

The construction of the novel single-crystalline SbSI nanorods array - WO_3 heterostructure photoanode for high PEC performance

Guoliang Peng, [a,b] *Huidan Lu,* [a,b] *Yongping Liu,* [a,b,*] *Dayong Fan,* [a,b,*]

[a]College of Chemistry and Bioengineering,

Guilin University of Technology, Guilin 116023, China

[b]Guangxi Key Laboratory of Electrochemical and Magneto-chemical Functional Materials, Guilin University of Technology, Guilin 541004, China.

Corresponding Authors: Dayong Fan & Yongping Liu

E-mails: dyfan@glut.edu.cn.& liuyp624@163.com.

Outlet

1. Experimental Section

1.1 Sample Fabrication

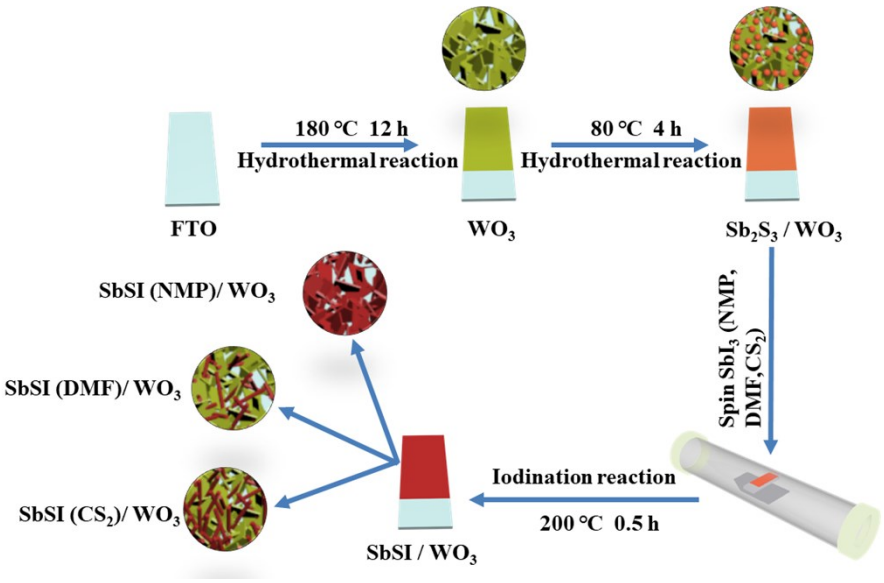

Scheme S1. The 4-step fabrication process for $SbSI/WO_3/FTO$ photoanodes

A hydrothermal method was used to prepare WO_3 using high purity $Na_2WO_4{\cdot}2H_2O$ (Xilong Scientific Co., Ltd. China, 99.5%), $C_2H_2O_4{\cdot}2H_2O$ (Xilong Scientific Co., Ltd. China, 100%). A typical process is as follows: weigh 2.4 g of $Na_2WO_4{\cdot}2H_2O$ and 0.2 g of $C_2H_2O_4{\cdot}2H_2O$ and dissolved them with 85 ml of distilled water in a beaker. After stirring for 3 hours, add 2.8 ml of 12 mol/L hydrochloric acid and stir for another five minutes. The solution was equally divided and transferred into two 50 ml Teflon-lined autoclaves in which a FTO glass fully immersed and put the sealed autoclaves in an oven at 180℃ for 12 hours. Take them out and rinse with distilled water several times. After drying, put them in a muffle furnace at 500℃ and calcined for 2 hours.

Hydrothermal synthesis of Sb_2S_3 on WO_3/FTO: Weigh and add 0.9125 g of $SbCl_3$ (Sino Reagent Co., China, 99.0%) and 0.744 g of $Na_2S_2O_3$ (Sino Reagent Co., China, 99.0%) into an 80 ml beaker in turn and stir for 15 minutes and 30 minutes, respectively. Divide the solution equally into two portions and put them into two 50 ml Teflon-lined autoclaves contained with the former WO_3 substrates. Put it in an oven at 80℃ for 4 hours, followed by rinsing with distilled water several times and drying.

The construction of $SbSI/WO_3$ photoanodes are iodized from Sb_2S_3/WO_3 involved with various solvents: Dissolved 0.15 g of SbI_3 (Sigma Aldrich, 99.998%) in 1 ml of N-methyl-2-pyrrolidone (NMP) (Sino Reagent Co., China, 99.0%) / in 1 mL N,N-Dimethylformamide(DMF) (Xilong Scientific Co., Ltd. China, 99.5%) or dissolved 0.02 g of SbI_3 in 0.5 ml of CS_2 (Rhawn Reagent Co., Ltd, China, 99.0%). After the dissolution was completed, used a pipette to take 30 μl of the solution and spin coat it on a Sb_2S_3/WO_3 substrate. After drying, calcined it in a tube furnace filled with nitrogen at 200℃ for 30 minutes.

A short illustration for the photoanode fabrication is depicted in Scheme S1.

1.2 (Photo-)Electrochemical Testing

The photoanodes were immersed in the electrolyte of 0.5M Na_2SO_4 aqueous solution (or others with specific descriptions in the text), using CHI660e model in the three-electrode configuration (a Pt wire as the counter electrode and a saturated Ag/AgCl electrode as the reference) equipped with a flat quartz-glass window. In two-electrode configuration, the LSV scan in the electrolyte of 0.5M Na_2SO_4 aqueous solution with a Pt wire as the counter electrode. For electrochemical impedance spectroscopy (EIS), E (V) = 0.5, high Frequency (Hz) = 10^5, low Frequency (Hz) = 0.1, Amplitude (V) = 0.005. For the linear-sweep voltammetry measurements, a chopped white light source with the calibrated output intensity of 100 mW/cm^2, simulating AM 1.5 G condition. In Mott-Schottky measures, the samples were tested in the Na_2SO_4 solution (pH 6.5) with the frequency of 1 kHz. And Incident Photon-to-electron Conversion Efficiency (IPCE) was measured in a home-made system containing a 300 W Xe lamp equipped with a calibrated monochromator.

1.3 Structural, Morphological and Optical Characterization

X-ray diffraction patterns were collected on a Philips X'Pert diffractometer using Cu Kα1 radiation with an anode current of 35 mA and an accelerating voltage of 40 kV over the angle range 2θ = 15 to 70°, scan rates 5^o /min. The scanning electron microscopy images and elemental analysis were collected using SU7000 (Hitachi Co., Ltd.), equipped with X-ray spectroscopy (EDS) attachment (SEM, JSM-638OLV). The transmission electron microscopy (TEM) images, high-resolution TEM and SEAD pattern were collected by JEM-2100F (JEOL Ltd.). The UV–vis absorption spectra of the as-obtained samples were measured by a UV/VIS/NIR Spectrometer

(PerKinElmer, Lambda 750) in the range of 200 to 800 nm. $BaSO_4$ was used as the reflectance standard material.

2. TEM, HRTEM and SEAD Analysis on SbSI(CS_2)/WO_3

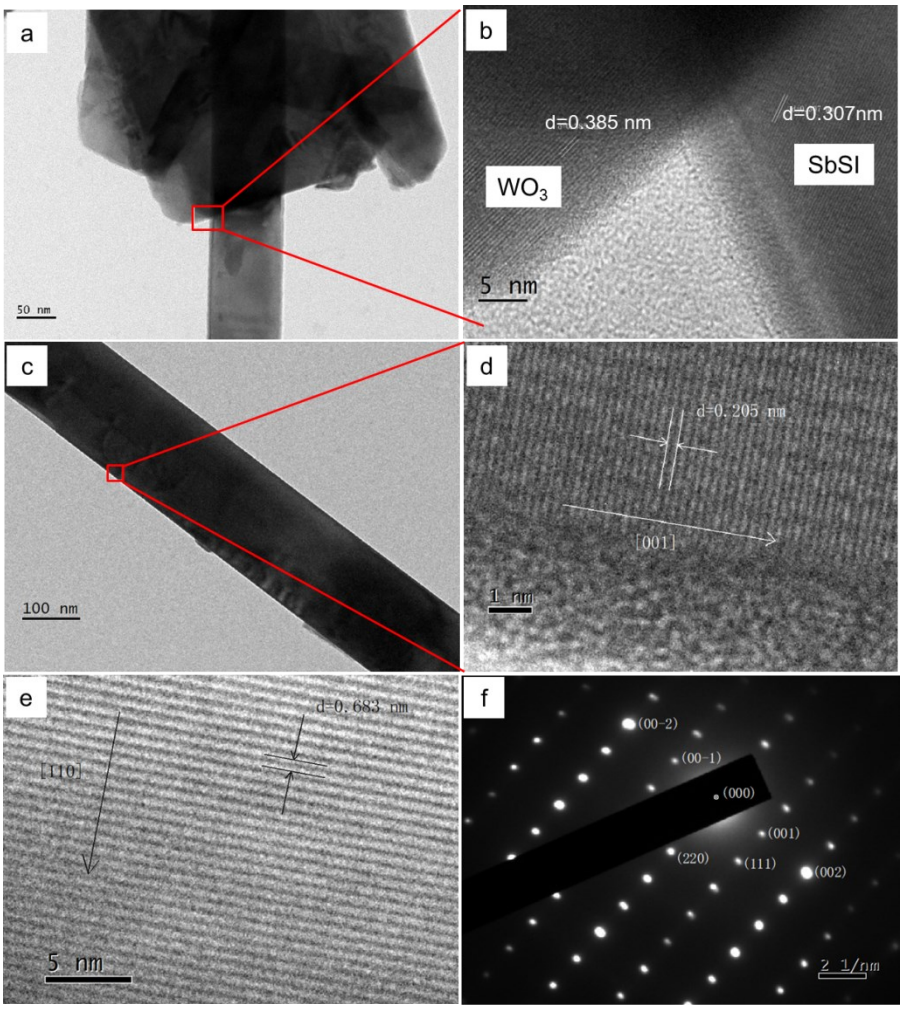

Figure S1. (a, b) The TEM and HRTEM images of WO_3 and SbSI stripped from a SbSI(CS_2)/WO_3 anode. Typical TEM of individual SbSI nanorod(c) and HRTEM images on specified area (d, e) shows the single SbSI nanorod grows in [001] direction, which is the polar direction of SbSI. f) Electron diffraction pattern shows a single crystal feature.

The monoclinic phase WO_3 nanoplates was confirmed further by the fringe spacing d=0.385 nm, indexed to the (001) planes of WO_3 ($P2_1/a$). Given d=0.307 nm, which corresponds to the (121) planes spacing of SbSI ($Pna2_1$), suggests the SbSI nanorods is in orthorhombic phase. To clarify the crystal structure and growth direction of SbSI nanorods, the HRTEM images and SEAD pattern of a single SbSI nanorod are given in Fig. S1c-f. From Fig S1d, the fringe spacing d=0.205 nm, which is exactly perpendicular to the nanorod growth direction, corresponds to the interplanar spacing of (002) planes in SbSI. This means the SbSI nanorods grow along [001] direction on the WO_3 nanoplates, which is the polar axis in ferroelectric state, make this structure valuable for studying ferroelectric effects further. For now, this topic is out of the scope in this paper. The SEAD pattern (Fig. S1f) revealed the SbSI nanorod is in a good single crystalline structure.

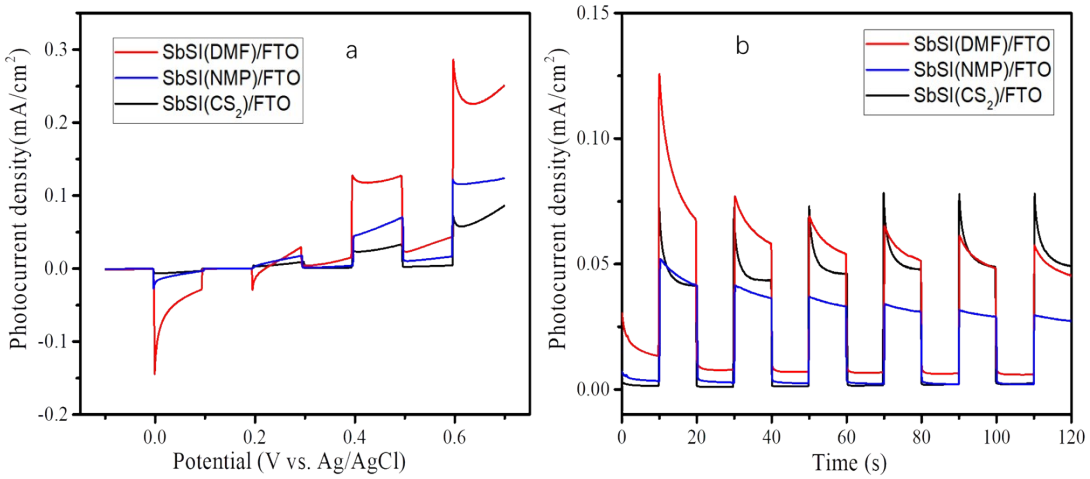

Fig. S2 (a) linear sweep voltammetry under chopped irradiation measured in 0.1 M Na_2SO_4 (scan rate: 10 mV/s); (b) photocurrent density−time curves at an applied potential of 0.50 V vs Ag/AgCl under illumination with 10 s light on/off cycles of SbSI(CS_2), SbSI(NMP) and SbSI(DMF).

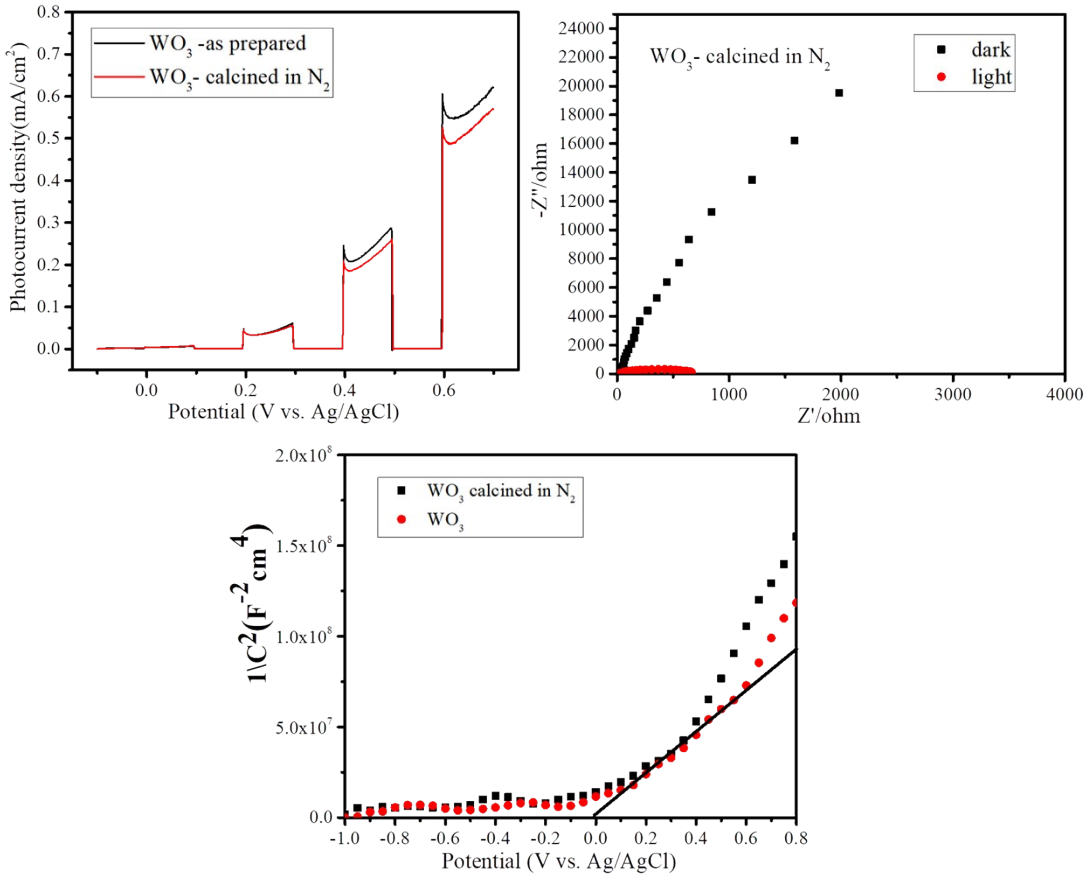

Fig. S3 The calcined WO_3 in nitrogen show little difference (< 0.05 mA/cm² @ 0.5 $V_{Ag/AgCl}$, upper left) in photoanodic current density, flat-band position and donor density (down) compared to the as-prepared one, while the impedance under irradiation is two-magnitude larger than the impedance in dark(upper right), indicate the WO_3 remain its intrinsic n-type semiconductor characteristic after calcination at 200 °C in nitrogen for 30 min.

3. The flat-band position dependence on pH

The dependence of flat-band potential on pH values of electrolyte are also measured by M-S analysis and given in Fig. S4. The fitting result follows a linear relationship (Fig. S5): V_{fb}=0.06-0.02*pH (vs. Ag/AgCl), which deviates from the Nernst equation (-0.059V/pH). Note that the slopes of M-S curves are also strong pH-dependent parameters (Fig. S4), which indicate the interface of semiconductor and electrolyte is sensitive to the concentration of proton or hydroxide in the electrolyte, owing to ion adsorption/desorption process.

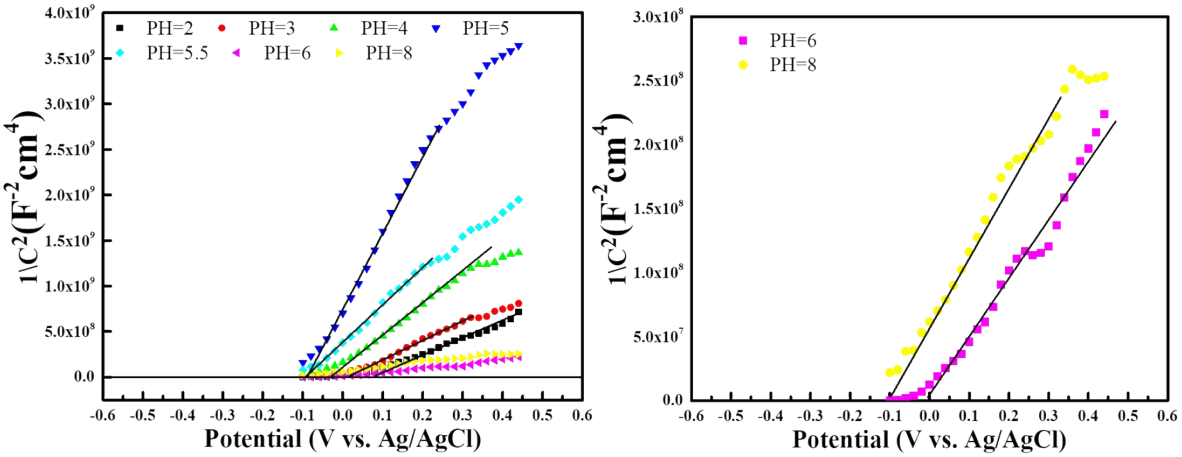

Fig. S4 M–S plots of $SbSI(CS_2)/WO_3$ in buffer solutions of pH from 2.0 to 8.0(d, e)

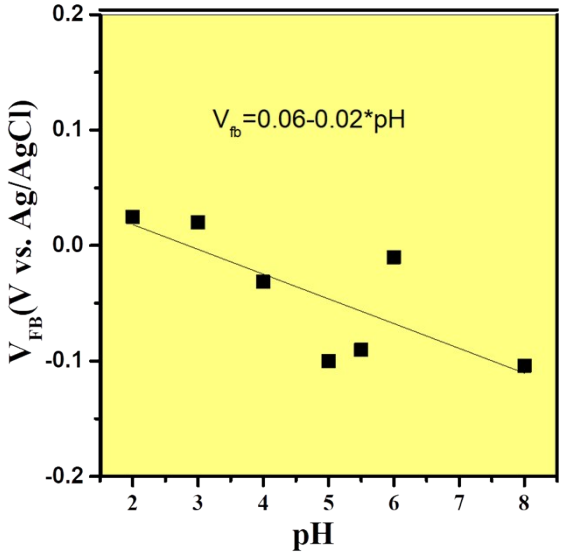

Figure S5. Linear fitting of flat-band potentials of $SbSI(CS_2)/WO_3$ (vs. Ag/AgCl) at various pH in aqueous solution.

4. Discussion on band alignment of the SbSI/WO_3 heterojunction photoanode

By analyzing the M-S curves further, it was calculated (Table S1) that the SbSI samples possessed low charge carrier densities ($N_d \sim 10^{17}$ cm^{-3}), which could be regarded as good quality crystals. In contrast, WO_3 possessed four-magnitude heavier donor density ($N_d \sim 10^{21}$ cm^{-3}) than SbSI, which would make SbSI act like an intrinsic semiconductor: the limited-density electrons thermally excited from donors in SbSI were incapable to migrate into WO_3 side for varying the overall flat-band potential of SbSI/WO_3, although the flat-band potential of SbSI is more negative than that of WO_3. This may be the reason that WO_3 could dominate the flat-band potential of anode constructed by SbSI and WO_3 heterostructure, and remain the shape of semiconductor-liquid interface.

Here the Fermi levels (E_F) of WO_3 and SbSI are estimated, based on the flat-band potentials (E_{fb}) obtained from M-S measurements, i.e. $E_f \approx E_{fb}$. Owing to the high donor density in WO_3, it is reasonable to suppose the flat-band potential is very near to the conduction band (CB) bottom. In addition, the relative position of E_c-E_f in SbSI were estimated and given in Table S1 (the calculation refers to the supporting information). Considering the Uv-vis diffusion spectra of SbSI and WO_3 anode, which indicate the bandgaps are 2.0 eV and 2.75 eV, respectively (Fig. 4a),

Table S1. The M-S analysis results of the WO_3, SbSI, SbSI(CS_2)/WO_3, SbSI(NMP)/WO_3 and SbSI(DMF)/WO_3 anodes

	N_d(cm^{-3}) [a, b]	V_{fb}(vs. RHE)	E_c-E_f(eV) [b]
WO_3	9.21×10^{21}	0.62	/
SbSI(NMP)	1.18×10^{17}	0.23	0.135
SbSI(CS_2)	3.11×10^{17}	0.23	0.111
SbSI(DMF)	4.54×10^{17}	0.23	0.101
SbSI/WO_3 for all	/	0.62	/

[a]. Calculated with the dielectric permittivity (ε_r=50) of WO_3[1]; [b]. Calculated with the c-axis dielectric permittivity (ε_r=50,000 at T=22°C) and effective electron mass ($m_e^*=0.21m_0$) of SbSI.[2-4]

Flat-band position and donor density calculation

The flat-band position (ϕ_{fb}) of unpoled SBN-50 can be inferred from Mott-Schottky relation:

$$\frac{1}{C_{sc}^2} = \frac{2}{N_d e \varepsilon_o \varepsilon_r}\left(\phi - \phi_{fb} - \frac{k_b T}{e}\right)$$

which is equal to the intercept of the M-S plots (Figure 4a). The flat band ϕ(NHE) can be converted to ϕ(RHE) from the relationship:

$$\phi(\text{RHE}) = \phi(\text{Ag/AgCl}) + 0.0591 \times \text{pH} + 0.197 \text{ (V) at 25℃}$$

From the slope of the $1/C_{sc}^2$ vs. E, the donor density (N_d) value of electrodes was estimated by:

$$K = \frac{2}{N_d e \varepsilon_o \varepsilon_r}$$

The calculation for effective density of states at the conduction band (N_c) and conduction band position (E_c)

The effective density of states of SbSI at the conduction band was calculated with the formula[5](not consider the quantum confinement effect):

$$N_c^{3D} = \frac{1}{\sqrt{2}}\left[\frac{m^* kT}{\pi\hbar^2}\right]^{3/2}$$

N_c=2.42×10^{18} cm^{-3} for SbSI, with effective electron mass m^*=0.24m_0.[3]

The relative offset between conduction band bottom (E_c) and Fermi energy position (E_f) could be estimated by[4]:

$$E_C - E_F = kT \cdot \ln\left(\frac{N_c}{n_0}\right) \approx kT \ln\left(\frac{N_c}{N_d}\right)$$

Given T=295 K, Boltzmann constant k = 8.6173×10^{-5} eV/K

Table S2. The fitting results of the equivalent circuit in impedance measurements with a series resistance (R_S), the semiconductor/electrolyte charge transfer resistance (R_{CT}), and bulk capacitance, CPE

Photoanodes	R_s/Ω	R_{ct}/Ω	CPE-T/F	CPE-P
WO_3	28.03±0.42	595.9±17.78	$1.1351*10^{-4}$±$6.9927*10^{-6}$	0.91837±0.012
Error %	1.49	2.98	6.16	1.35
SbSI	18.31±0.32	8410±172.23	$1.066*10^{-5}$±$3.7565*10^{-7}$	0.95398±0.0057
Error %	1.72	2.05	3.52	0.60
SbSI(NMP)/WO_3	68.33±0.98	384±15.55	$5.1082*10^{-4}$±$4.0418*10^{-5}$	0.82533±0.022
Error %	1.44	4.05	7.91	2.67
SbSI(DMF)/WO_3	31.68±0.35	690.6±17.96	$1.9415*10^{-4}$±$8.4167*10^{-6}$	0.85187±0.0094
Error %	1.10	2.60	4.34	1.10
SbSI(CS_2)/WO_3	35.55±0.63	506.4±19.36	$3.2482*10^{-4}$±$2.271*10^{-5}$	0.90329±0.018
Error %	1.76	3.82	6.99	1.97

5. **Discussion on Photostability of SbSI/WO_3** photoanodes

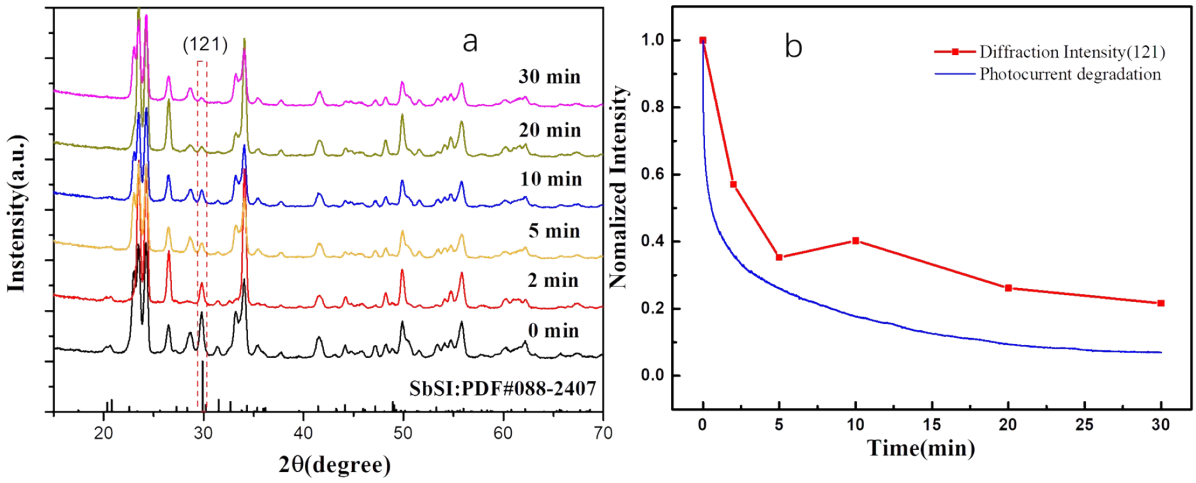

Figure S6. a) The XRD patterns of a SbSI(CS_2)/WO_3 photoanode after a certain period of photoanodic reaction in Na_2SO_4 solution at 0.5V(vs. Ag/AgCl); b) normalized diffraction intensity curve of (121) plane belong to SbSI and photocurrent with reaction time in the same condition.

For investigating the reason of photocurrent degradation, we monitored the XRD spectra of a SbSI(CS_2)/WO_3 photoanode during the reaction was processing(Fig. S6a). As indicated, the peak belongs to (121) diffraction plane is the representative one for monitoring the status of SbSI phase on the photoanode, since it is the most intensive peak in standard XRD pattern of SbSI. As prolonging the reaction time, the intensity of (121) peak decreases significantly, while no extra diffraction peak was detected on the pattern. The peaks which belong to WO_3 are almost unchanged. At the same time, we observed the color change of SbSI(CS_2)/WO_3 by eyes: The dark red on the anode gradually fade away during the reaction process. Taking into account of the consistent relationship betwteen normalized diffraction intensity of (121) and photocurrent with reaction time (Fig. S6b), we could speculate: on the one hand, the falling of SbSI from the anode is the main reason of photocurrent degradation; on the other hand, there is no solid crystallized product generated during the photoanodic process. Instead, quite possibly, the main by-products enter in the electrolyte by the means of soluble ion. The solution after reaction was further analyzed by inductively coupled plasma-optical emission spectrometry (ICP-OES) method, in which the Sb element was detected. A comparative experiment for clarify the potential degradation mechanism was performed, which shows that the sample degrade significantly when preserved in a high humidity environment, but much better in an oven or in n-hexane (Fig. S7, S8). Due to the high cumulative formation constants, some Sb(III)-hydroxide complexes may be the oxidation products, such as[6]:

$Sb^{3+}+2OH^- = Sb(OH)_2^+$ $\log K_2 = 24.3$

$Sb^{3+}+3OH^- = Sb(OH)_3$ $\log K_3 = 36.7$

$Sb^{3+}+4OH^- = Sb(OH)_4^-$ $\log K_4 = 36.7$

In this respect, it is easy to understand the fact: SbSI was observed easily to dissolve in the alkaline condition or to be corroded under anodic process.

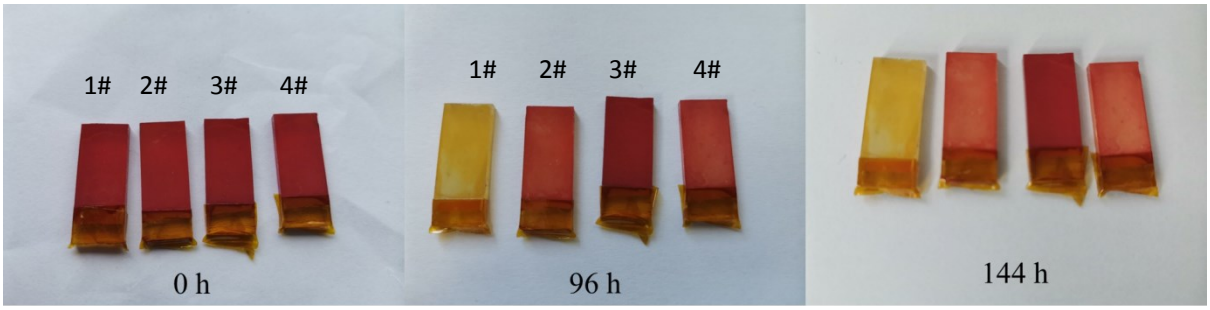

Fig. S7 For investigating the SbSI in moisture and air, we preserved four groups of fresh $SbSI(CS_2)/WO_3$ for a period time in various environments for comparison.

(From left to right) #1: exposed in ambient atmosphere with air; #2: immersed in distilled water. #3: preserved in an oven with 60°C; #4: immersed in water gas-filled with nitrogen.

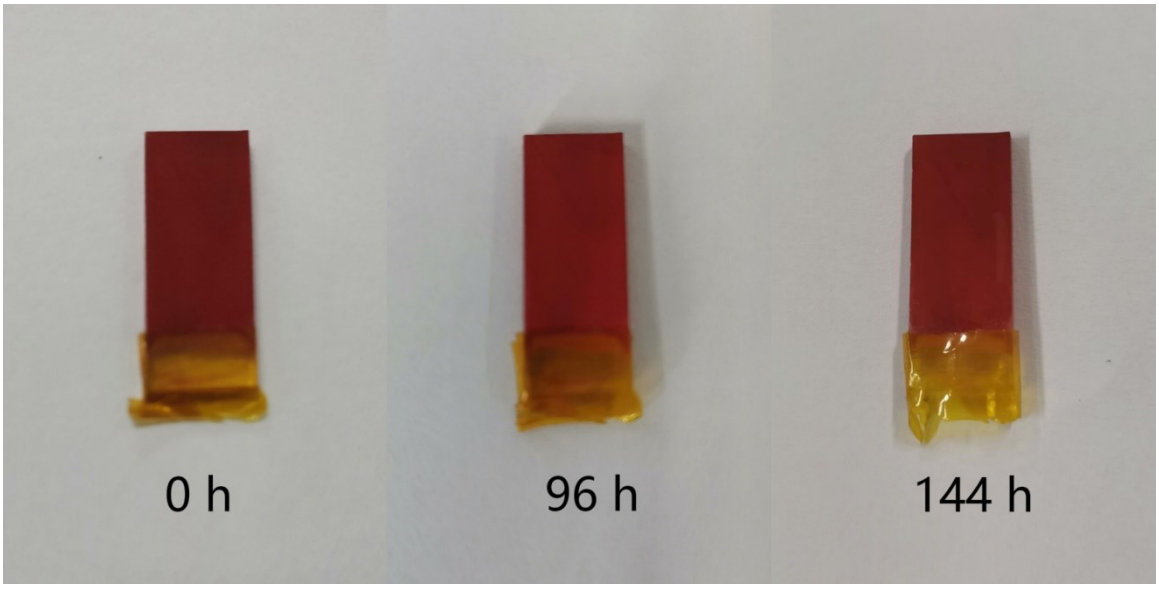

Fig. S8 The $SbSI(CS_2)/WO_3$ photoanodes preserved in pure n-hexane in different duration, which showed a much better stability than that in water.

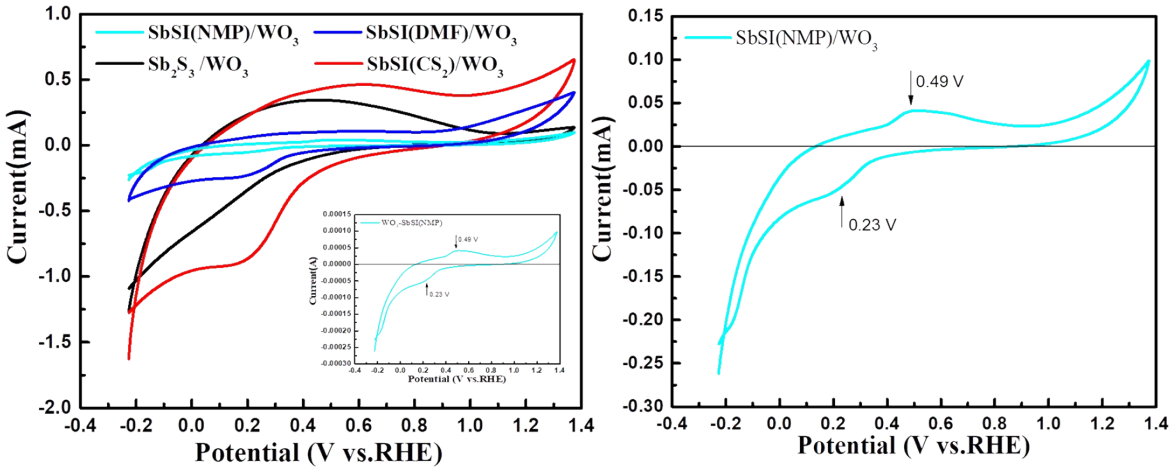

Fig. S9 The cyclic voltammograms of $SbSI/WO_3$ in dark, recorded in 0.1 M Na_2SO_4 solution, sweeping rate 10 mV s^{-1}.

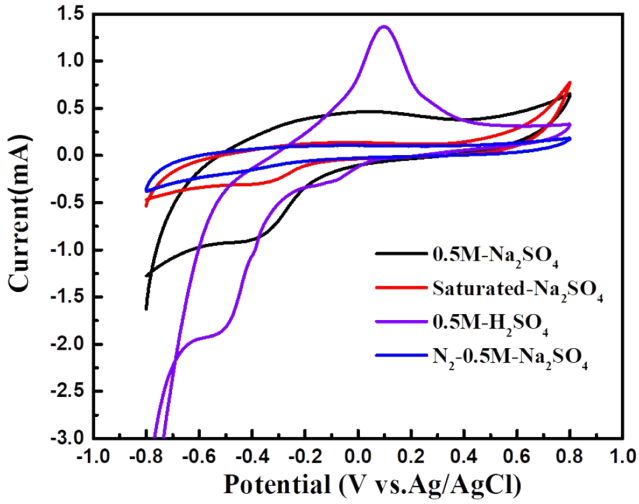

Fig. S10 The cyclic voltammograms of $SbSI(CS_2)/WO_3$ recorded in 0.5 M Na_2SO_4, saturated Na_2SO_4, 0.5 M H_2SO_4 and nitrogen-filled 0.5 M Na_2SO_4 solution, sweeping rate 20 mV s^{-1}.

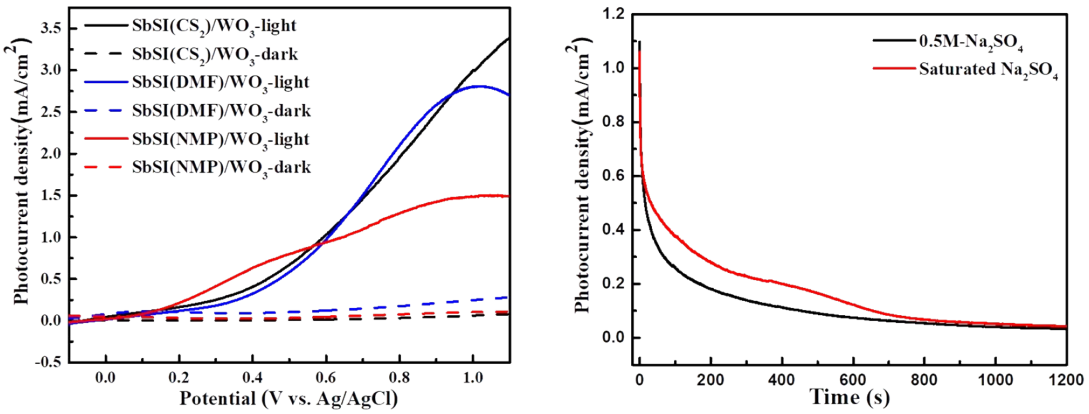

Fig. S11 (left) LSV curves of $SbSI/WO_3$ measured in saturated Na_2SO_4 under dark and light; (right) Comparison for photostability of $SbSI(CS_2)/WO_3$, with applied bias of 0.5 V vs. Ag/AgCl.

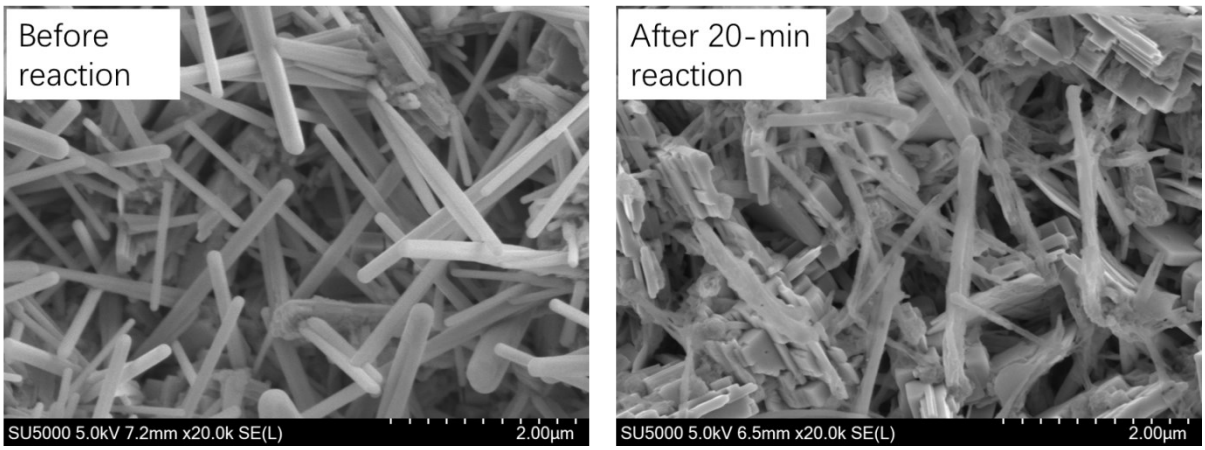

Fig. S12. SEM comparison of $SbSI(CS_2)/WO_3$ before and after reaction

6. References

1. N. Gaillard, Y. Chang, A. DeAngelis, S. Higgins and A. Braun, *International Journal of Hydrogen Energy*, 2013, **38**, 3166-3176.
2. E. Fatuzzo, G. Harbeke, W. J. Merz, R. Nitsche, H. Roetschi and W. Ruppel, *Physical Review*, 1962, **127**, 2036-2037.
3. K. T. Butler, J. M. Frost and A. Walsh, *Energy & Environmental Science*, 2015, **8**, 838-848.
4. D. Neamen, *Semiconductor Physics And Devices*, McGraw-Hill Education, 2003.
5. T. Edvinsson, *R Soc Open Sci*, 2018, **5**, 180387.
6. J. A. Dean and N. A. Lange, *Lange's Handbook of Chemistry*, McGraw-Hill, 1992.